Available online at www.sciencedirect.com

ScienceDirect

journal homepage: www.elsevier.com/locate/he

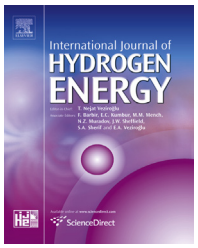

Effect of intermediate nickel layer on seal strength and chemical compatibility of glass and ferritic stainless steel in oxidizing environment for solid oxide fuel cells

M. Fakouri Hasanabadi, A. Nemati[*], *A.H. Kokabi*

Department of Materials Science and Engineering, Sharif University of Technology, Azadi Avenue, P. O. Box 11155-9466, Tehran, Iran

ARTICLE INFO

Article history:
Received 27 March 2015
Received in revised form
2 September 2015
Accepted 1 October 2015
Available online 28 October 2015

Keywords:
Solid oxide fuel cell
Nickel plating
Stainless steel
Glass
Seal

ABSTRACT

The effects of intermediate nickel layer on seal strength and chemical compatibility of seal glass and interconnect materials for solid oxide fuel cells (SOFCs) were investigated. Two types of samples (metal/glass/metal sandwiches and glass coated metals) were prepared with the sheet of AISI 430 (nickel plated and uncoated) and slurry of compliant silicate sealing glass (SCN-1). The joined and coated samples were heated at 850 °C for different time durations (0.5–100 h). Tensile and impact tests were performed and SEM micrographs were used to analyze the glass/metal interaction. The results indicate that nickel plated AISI 430 shows higher adhesion strength at short durations of heating due to dendrite development at the interface. For longer durations, intermediate nickel layer leads to rapid loss of adhesion strength due to extension of unstable austenite zones but prevents the accelerated weakening near the triple-phase boundaries metal/glass/air (TPB) by compensating for absence of protective oxide layer (Cr–Mn oxide).

Introduction

Solid oxide fuel cells (SOFCs) are emerging technologies for direct conversion of fuel to electricity. SOFCs are considered as alternative systems for generating electric power due to their interesting features such as high energy-conversion efficiency, fuel flexibility, environmental safety, low noise and ability to recover exhaust heat [1–3]. One of the major challenges for commercializing SOFCs, especially planar-SOFCs, concerns sealant materials. These sealants must prevent fuel–oxidant mixing and provide electrical insulation of the stack layers for long times (5000–40,000 h) at high temperatures (between 600 °C and 1000 °C) [4,5]. Several approaches have been used to seal SOFCs including compliant (viscous) seal, compressive (soft) seal and rigidly bonded (semi-rigid) seal [6–8]. Glasses and glass-ceramics (GCs), especially the silica-based ones, have been extensively studied in all three approaches due to achievable good properties such as low electrical conductivity, compatible coefficient of thermal expansion (CTE), good adhesion and limited reactivity with SOFC components and atmospheres [6–11].

* *Corresponding author*. Tel.: +98 21 6616 5223; fax: +98 21 6600 5717.
E-mail addresses: fakouri@mehr.sharif.ir (M. Fakouri Hasanabadi), nemati@sharif.edu (A. Nemati), kokabi@sharif.edu (A.H. Kokabi).
http://dx.doi.org/10.1016/j.ijhydene.2015.10.023

A determining factor affecting the durability of SOFCs is the interaction of glass with interconnects. Ferritic stainless steel (FSS) is the most promising candidate for interconnect applications due to its low cost, good CTE match with electrolyte materials and high oxidation resistance [12]. Nevertheless, undesirable reactions between glass and FSS, especially near the air-side, can potentially lead to deleterious high expansion chromate formation, microstructure degradation and electrical shorting [13,14]. Therefore, it seems that further improvement in long-term stability is needed. On the other hand, chemical interactions are necessary to achieve a satisfactory glass/FSS adhesion during thermal cycling, especially below the glass transition temperature (T_g) when the glass is not soft [15–18]. For these purposes, in addition to modification of glass and FSS compositions [19–23], many efforts have been made on the modification of FSS surface including pre-oxidation [24,25], aluminizing [26–29] and applying protective coating [30–37].

Recently, nickel has been investigated as protective coating for AISI 430 and AISI 441 in order to reduce the rate of Cr evaporation and prevent the growth of semi-conductive Cr_2O_3 scale under SOFC conditions [38–41]. Also, it has been reported that Ni-oxide improves the adhesion and reduces the metal/glass interactions [30]. Although effects of intermediate nickel layer between steel and glass are very well-known in porcelain enameling industry for many years [42–44], the details of its behavior in SOFC conditions are not available.

The purpose of this study was to provide a better understanding of chemical interaction of glass/metal adhesive joints with/without intermediate nickel layer. The impact test was used to validate the low strain rate tensile test for SOFC sealing applications. Also, SEM micrographs were analyzed based on prior knowledge about the glass/metal interactions (corrosion, enameling, glass coloring and …). SCN-1 as a non-crystallizing compliant sealing glass allows us to focus on interfacial interactions for seal strength investigation.

Experimental

Materials and sample preparation

Commercial alkali silicate glass (SCN-1, Par-e-tavous, Khorasan-e-razavi, Iran) was used. This silicate glass contains alkaline earth elements, mainly in the form of BaO (8.23 mol %) and CaO (3.34 mol%), alkalis of K_2O (10.0 mol%) and Na_2O (7.3 mol%), Al_2O_3 (2.8 mol%), and some impurities (less than 1%) of Fe, Mg and Ti with the balance of SiO_2. T_g, softening point (T_d), and CTE were about 470 °C, 550 °C and 11×10^{-6} °C^{-1}, respectively. The details of glass composition and its thermal behavior with AISI 441 are available in the literature [17,28,33,45].

AISI 430 is a commercial ferritic stainless steel (Hardox, Oxelösund, Sweden) containing Cr (17.5 wt%), Ni (0.13 wt%), C (0.05 wt%), Mn (0.25 wt%), Cu (0.13 wt%) and Si (0.15 wt%) with the balance of Fe. In this study, AISI 430 sheets with a thickness of 0.5 mm were used in two states of Ni-plated and uncoated which are specified here by N and S, respectively. N sheets were prepared as follows; AISI 430 was abraded with #1200 grit abrasive paper, the surfaces were degreased with acetone and activated in Woods nickel strike solution and then nickel was electroplated using Watts solution until obtaining a thickness of around 10 μm. Each step was followed by water rinsing to remove chemical residues. The interactions between SOFC atmospheres and FSS have an important role in damage growth near the triple-phase boundaries metal/glass/air (TPB). The coating with thickness of 10 μm is chosen because it has been reported that FSS with 8–10 μm thick nickel coating performs better under SOFC atmospheres [38,41].

The glass was applied onto the AISI 430 surface by using a slurry method. The slurry was a mixture of glass powder and minor additives (borax, sodium nitrate, kaolin, and silica) dispersed in deionized water. Two types of samples were prepared: glass coated AISI 430 sheets with dimensions of 6×6 cm^2, for impact tests and AISI 430/glass/AISI 430 sandwiches (joined samples) with dimensions of 1×1 cm^2 for tensile tests. The thickness of glass in type one and two after joining was 0.4 ± 0.1 mm and 0.5 ± 0.05 mm, respectively. After applying the slurry, the samples were dried at 70 °C for 15 min. The dried samples were then thermally treated at 850 °C for different time durations (0.5–100 h) in air. The heating and cooling rates were about 9 °C/min and 2 °C/min, respectively. The code of the samples was based on the surface condition of AISI 430 sheet and heat treatment duration; For example, N1 was assigned to a sample with Ni-plated sheet which was heat treated for 1 h.

Mechanical testing and microstructural characterization

Impact test was performed in accordance with a modification of EN 10209 Annex D method in ambient conditions [46]. In this method, a punch with hemispherical tip hits glass coated sheet and the adhesion strength is evaluated based on the destroyed surface appearance. For quantifying the results, the percent of bare areas which is inversely proportional to the adhesion level was calculated with the aid of the ImageJ software (version 1.46) [47]. For seal strength tests, the joined samples were glued to two aluminum test fixtures by cyanoacrylate (as shown in Fig. 1). The fixture had a self-alignment joint to minimize bending or twisting during tensile testing. Detailed information about test principles and equipment is described in Refs. [24,48]. The assembly was then tested in uniaxial tension with a cross-head speed of 0.5 mm min^{-1} in ambient conditions. For each condition, 4 samples were tested, the outlier was discarded, and the average strength was determined. Some of the samples were also mounted in epoxy and then sectioned and polished for interfacial characterization using optical (Olympus BX51M) and scanning electron microscopes (SEM VEGA\\TESCAN-XMU and FE-SEM TESCAN MIRA3 LM).

Results and discussion

Seal strength

Fig. 2 shows the room temperature seal strengths of AISI 430/glass/AISI 430 joined samples as a function of heating duration. Fracture surface analysis revealed that crack propagation

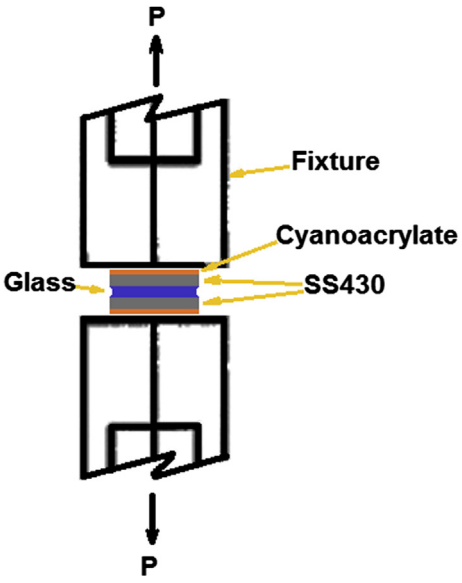

Fig. 1 – A schematic drawing showing the tensile testing assembly with a joined sample bonded to the grips with glue (cyanoacrylate).

mainly occurs along the glass/metal interface. It means that adhesion of glass/metal controls the seal strength. Results of impact tests are shown in Fig. 3. Although relative mechanical behavior of some samples was different in the two tests, general trend of relation between time duration and adhesion strength was the same. At short durations, adhesion tends to increase with an increase in the heating duration due to the development of an interface transitional layer compatible with both glass and metal, as reported earlier [7,44].

Fig. 4 shows that the interdiffusion distances at the interface in N1 sample, which has the highest adhesion strength, is about the same of those for S1 sample. These interdiffusion distances can provide the same transition layer but there are two reasons that explain why N samples have higher adhesion strength than S samples, at short durations.

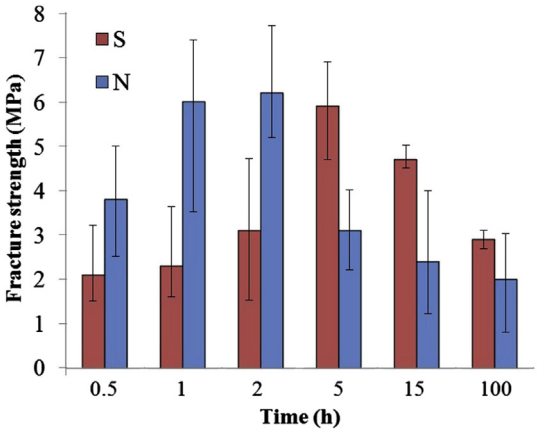

Fig. 2 – The room temperature seal strengths of AISI 430/glass/AISI 430 joined samples as a function of heating duration.

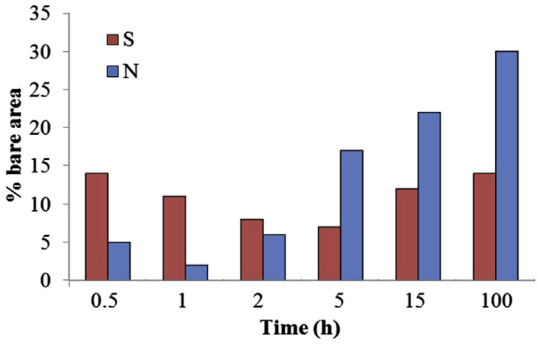

Fig. 3 – Percent of bare area on the samples after impact testing as function of heating duration.

First of all, the main adhesion mechanism of glass to chrome containing steels includes formation of an adherent and continuous oxide layer (Cr–Mn oxide) on these steels. This oxide layer increases the wettability of the glass on the AISI 430 and decreases the CTE mismatch between them [7,21,25,49]. Exposure to the air causes the formation of a weak Fe-rich oxide on the AISI 430 surface before glass softening which delays the formation of a suitable oxide layer and thus adhesion development. Secondly, as it is shown in Fig. 5(a) and (b), SEM micrograph of N1 represents the formation of some metal oxide-rich dendrites close to the interface which are not observed in S1. In Fig. 5(a), label B indicates the valley formation due to non-uniform dissolution of Ni-coating during heating, and label A indicates dendrite formation as a result of non-uniform precipitation of dissolved Ni during cooling. This phenomenon is more obvious near TPB and will be explained in Section chemical compatibility. The dendritic structure improves the mechanical interlocking and also increases the interface toughness.

At longer duration, adhesion strength decreases gradually. In S samples, glass gradually infiltrates through the Cr–Fe–Mn oxides rich layer [25] and results in the separation of the adherent oxide layer (Cr–Mn oxide) from the AISI 430 surface (Fig. 6). On the other hand, the traces of glass near the edge of AISI 430 after tensile testing become lower with increasing the duration from 1 h to 100 h. It means that the interfaces near the TPB become significantly weaker with increasing the duration. Seal strength is very sensitive to any weak points but the weakness of TPB does not affect the results of impact test, because the impact affected surfaces are away from these regions. Based on these arguments, Figs. 2 and 3 demonstrate that intermediate nickel layer prevents the accelerated weakening near the TPB but leads to rapid loss of adhesion strength away from these regions.

Fig. 7(a) shows the interdiffusion of elements near the interface in N15. According to the amounts of Cr, Ni and Fe elements in various areas, it is possible to introduce three zones near the interface: zone 1 in which, the amount of Ni, as an austenite stabilizer element, is high and the austenite phase becomes stable to room temperature, zone 2 in which Cr, as a ferrite stabilizer element, counteracts some effects of Ni and the austenite phase becomes stable to a temperature between T_g and room temperature, and zone 3 in which the

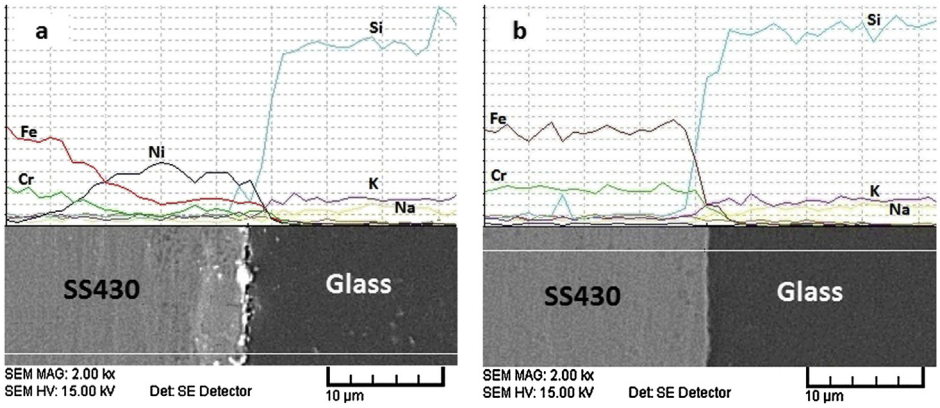

Fig. 4 – EDS line scan profile across the interface of (a) N1 and (b) S1.

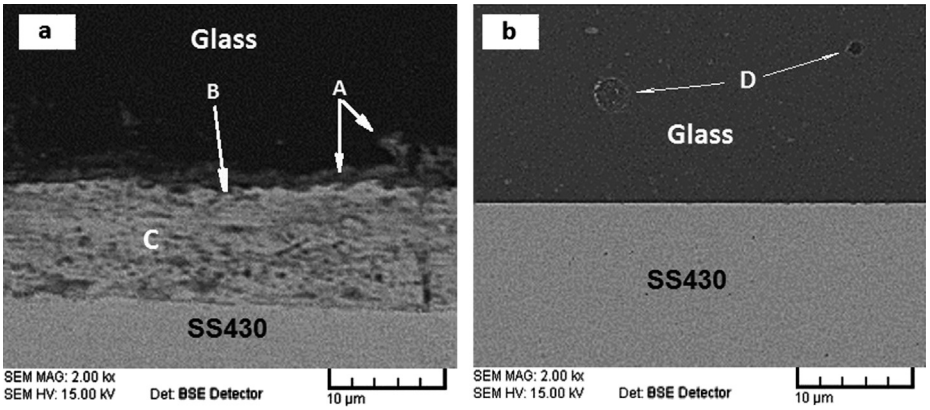

Fig. 5 – Cross-sectional backscattered electron microstructure of (a) N1 and (b) S1. A: Metal oxide-rich dendrite, B: Valley, C: Rich in Ni, Cr and Fe, D: Bubbles.

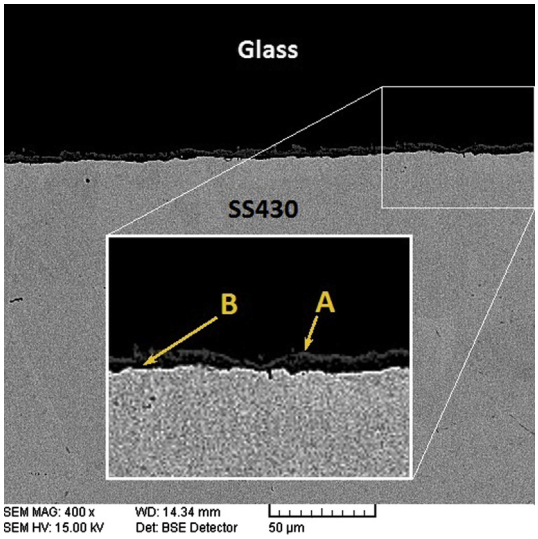

Fig. 6 – Cross-sectional backscattered electron microstructure of S100. A: Cr–Mn oxide B: Cr-rich glass.

amount of Ni is low and the austenite transforms to ferrite at temperatures above T_g [38,40,50]. These zones are shown in Fig. 7. The austenite to ferrite transformation is followed by a significant volume expansion in a short temperature range. In addition, an ejection of hydrogen is possible during the transformation due to higher solubility of hydrogen in austenite than ferrite [43,51]. The possible sources of hydrogen include the absorption during the electroplating and chemical reaction between the metal and the glass. The ejected hydrogen atoms can diffuse into glass/metal interface, and lead to increased gas pressure in the microcracks or gas bubbles formation [9,43,51]. Accordingly, in N samples, adhesion strength decreases with increasing the heating duration due to extension of zone 2 and zone 3 and also generation of inhomogeneous residual stresses at the interface during cooling.

Chemical compatibility

Fig. 8 shows the diffusion distances of Fe, Cr and Ni elements into the glass. The diffusion distance was considered

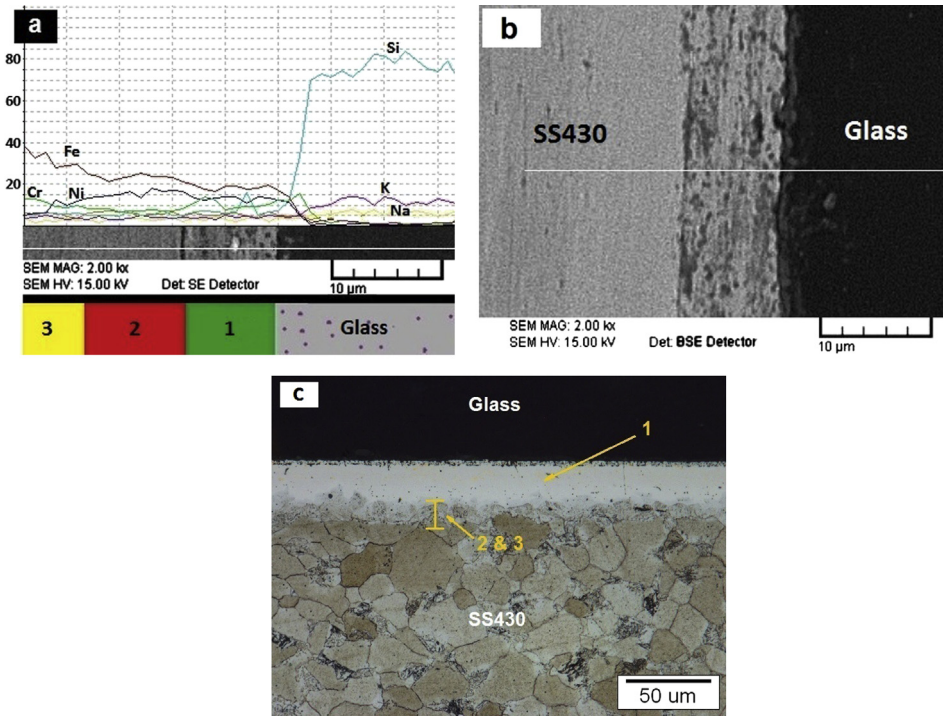

Fig. 7 – N15 sample; (a) EDS line scan profile across the interface, (b) Backscattered electron SEM micrograph, (c) Cross-sectional optical micrograph after etching with marble reagent. Zone 1 has austenite phase, and zone 2&3 is a mixture of ferrite (mustard) and austenite (bright white), and below them, there are the coarse grains of ferrite. Based on austenite stability, zones 1 to 3 are schematically shown.

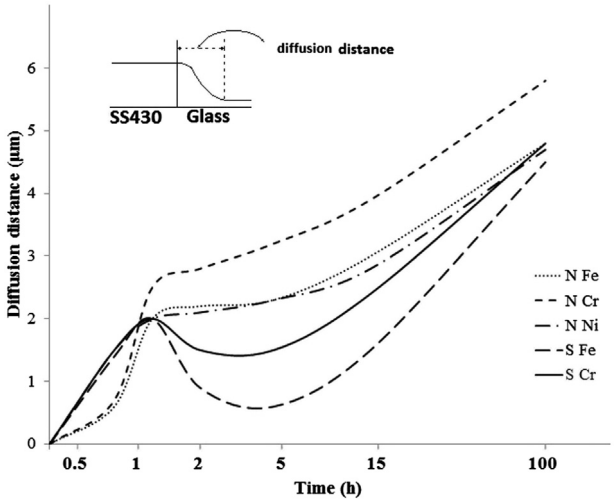

Fig. 8 – The diffusion distances of Fe, Cr and Ni elements into the glass as a function of heating duration. Method of measuring the diffusion distances is shown.

as the distance between the glass/metal interface and the point that the amount of element reaches about zero. After complete dissolution of the surface oxides into the glass, further progress of interaction depends on the oxygen activity at the interface, as mentioned by others [44,52]. The oxygen activity can be increased by reduction of the thermodynamically less stable components in the glass (and releasing the O^{2-} ions) or by diffusion of O_2 through some defects like cracks [44,53]. These two sources are not very active in viscous glass due to low speed ion transportation and self-healing behavior. Therefore, as it can be seen in Fig. 8, the rate of interaction tends to decrease with increasing the heating duration (note that log scale was used for horizontal axis).

As it is clear from Fig. 8, there is a decrease in diffusion distance curves in time range of 1–5 h for S samples. A large volume of Cr-poor (Fe-rich) oxide layer is formed on the surface of metal before glass softening. With decreasing the viscosity of glass, this layer is quickly dissolved in the glass [44]. During the heating procedure, Cr and Mn continuously diffuse into the interface and absorb the O^{2-} of the less stable oxides due to lack of access to atmosphere. Fig. 9 illustrates these competitive reactions; Cr pulls Fe_xO_y from the glass to the interface in order to absorb the oxygen (by redox reactions) but some of Fe_xO_y cannot recede. The knolls of residual Fe can be seen at a certain distance from the interface in EDS line scan across the interfaces of S5 and S15 samples (Fig. 9). The redox-type interfacial reactions can also be used to explain dendrite formation in N samples; Dissolved Ni-oxide can be reduced by Fe which has been diffused into the interface; Reduced Ni participates in form of dendrite and is alloyed with Fe at the interface [42,44]. The mentioned two redox reactions are shown in equations (1) and (2).

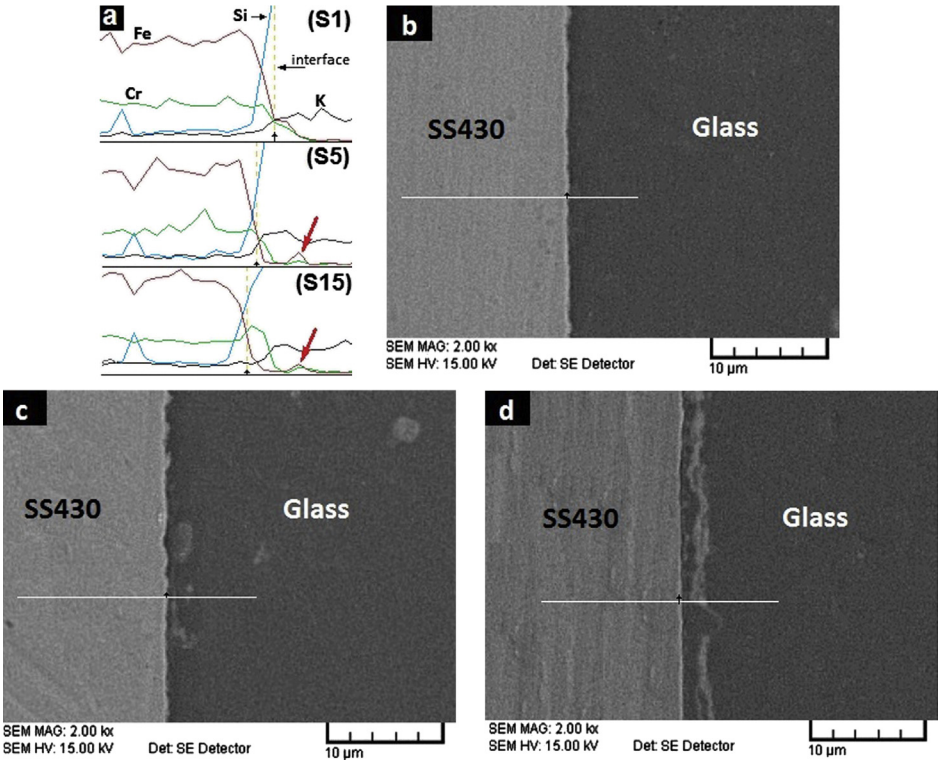

Fig. 9 – (a) EDS line scan profile across the interface for S1, S5 and S15, respectively (from up to down). The red arrows show the knolls of residual Fe. SEM micrographs of (b) S1, (c) S5 and (d) S15. (For interpretation of the references to color in this figure legend, the reader is referred to the web version of this article.)

$$n\ Cr + m\ Fe^{n+} => n\ Cr^{m+} + m\ Fe \quad (1)$$

$$k\ Fe + n\ Ni^{k+} => k\ Fe^{n+} + n\ Ni \quad (2)$$

where n, m and k are integers. This type of reaction is cause of interaction between glass-metal in the absence of oxygen (or metal oxides).

There is a second theory for dendrite formation which can also be used for explaining the interaction at the TPB. Based on this theory, dissolved metals in glass normally tend to crystalize during cooling through nucleation and growth procedure. According to thermodynamic principle, the dendritic solidification is a heterogeneous nucleation process and these nucleuses usually occur on the interface which is the reason why the dendrites exist as parts of metal substrate. More information in this regards is available in the literature [54,55]. The second theory is more appropriate because, based on first theory, the dendrites should be alloys without oxygen, but they are metal oxide-rich here.

The SEM micrograph of N100 and S100 samples (Fig. 10) shows a large volume of nodules (F) and dendrites (C) of metal-oxide near the TPB. Here, the activity of oxygen is high due to more access to atmosphere, thus the competition for oxygen is diminished. Nevertheless, the competitive reactions still continue for forming more stable structures [56,57]. Therefore, a large volume of different metal oxides can be continuously produced near the TPB and dissolved in glass. The metal oxides are dissolved in the glass through acid–base reactions. The acidic oxides such as silicate glasses can dissolve the basic or amphoteric oxides such as Fe_2O_3. This type of reaction is main cause of interaction between glass-metal in the presence of oxygen (or metal oxides) [44].

According to the second theory, this large volume of dissolved metals leads to formation of large volume of nodules and dendrites during cooling [29]. In addition, some reactions produce insoluble phases such as chromate [53,58]. The metal-rich oxides and the chromates have a high CTE that leads to damage growth during thermal cycling [14,28] and also electrical shorting in the cell stack [13,14,59].

Fig. 10 shows that damage growth in S100 sample near TPB is significantly more than in N100. In S samples, suitable oxide layer (Cr–Mn oxide) cannot form due to continuous oxidation and dissolution of metal surface at TPB. Internal oxidation (E) with the formation of chromia also leads to Cr depletion near the AISI 430 surface (zone H) and a local volume increase of chromia. This results in deterioration of corrosion resistance performance and delamination cracking along the interface between the glass and the AISI 430. Therefore, oxidation and dissolution of metals are accelerated near the TPB of S samples. In N samples, there is a semi-adherent oxide (Ni-oxide) on the surface of steel from the beginning that decelerates the oxidation and is a good barrier for formation of internal chromia and interfacial chromate [41]. In addition compared to Fe and Cr, Ni has a lower tendency to be dissolved in glass [60] due to lower tendency to absorb oxygen. Therefore, as it is seen in Fig. 10, the intermediate nickel layer can reduce the volume of damage zone at the interface to half.

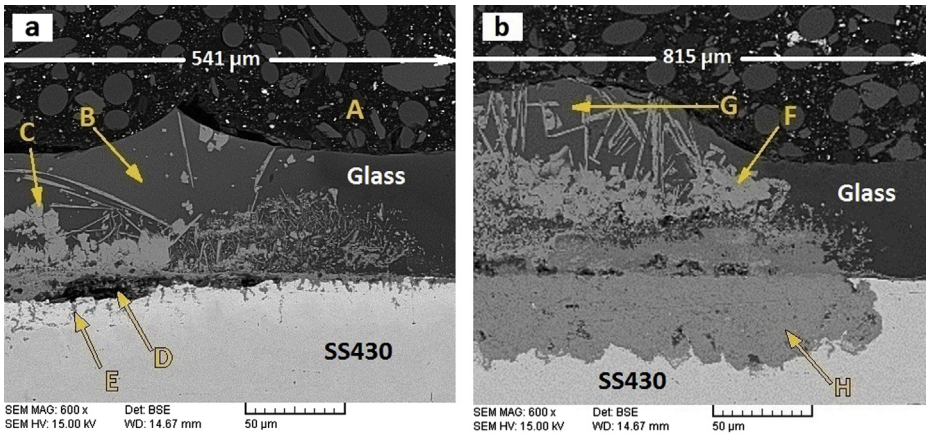

Fig. 10 – Backscattered electron SEM micrograph of TPB for (a) N100 and (b) S100. A: epoxy, B: Fe-rich glass, C: Fe–Ni oxide rich dendrites, D: cavity, E: Cr-oxide rich, F: Fe-oxide, G: Fe-rich glass, H: Fe–Cr oxide. The white arrow indicates the distance from the TPB.

Ni-coating seems to have two antithetic effects; 1) on damage growth near TPB, 2) on Low temperature adhesion strength. Depending on sealant nature, one of these effects can become negligible. For compliant or compressive sealants with high chemical activity and high self-healing capability at working temperature of SOFC, damage zone grows rapidly at the TPB and Ni-coating can be helpful. This damage zone reduces the effective interface for load bearing, induces some local stresses, and can lead to electrical shorting. In other words, the negative effect of Ni-coating on low temperature adhesion strength is negligible. But for rigidly bonded sealants with low chemical activity and also low self-healing capability, Ni-coating is harmful because the positive effect on damage zone growth at the TPB is negligible.

Conclusions

In this study, nickel was electroplated on the AISI 430 alloy as SOFC interconnect and the performance of the coating was evaluated as an intermediate layer between interconnect material and sealing glass at 850 °C for different time durations (0.5–100 h) in the air.

At short heating durations (less than 5 h), the uncoated samples (S samples) show lower adhesion strength than nickel plated samples (N samples). In the N samples, formation of a dendritic structure at the interface increases the mechanical interlocking and interface toughness.

Results of impact and tensile tests illustrate that at longer durations (5–100 h), the intermediate nickel layer leads to rapid loss of adhesion strength but prevents the accelerated weakening near the triple-phase boundaries metal/glass/air (TPB). Ni layer leads to extension of unstable austenite zones near the interface. The ferrite to austenite transformation during cooling generates some residual stress at the interface and thus reduces the adhesion strength. In the S samples, suitable oxide layer (Cr–Mn oxide) cannot form near TPB (due to continuous oxidation and dissolution of metal surface). Ni layer compensates the absence of Cr–Mn oxide at the TPB and decelerates damage growth.

Acknowledgments

The authors gratefully acknowledge Iran Board Electronic Company for providing the electroplating requirements, and support of Renewable Energy Organization of Iran (SUNA). We also express our gratitude to Dr. S. Banijamali, Miss S. N. Salimian and Miss E. Mohaghegh.

REFERENCES

[1] Aparicio M, Jitianu A, Klein LC. Advances in sol–gel derived materials and technologies. London: Springer; 2012.
[2] Tulyaganov DU, Reddy AA, Kharton VV, Ferreira JMF. Aluminosilicate-based sealants for SOFCs and other electrochemical applications – a brief review. J Power Sources 2013;242:486–502. http://dx.doi.org/10.1016/j.jpowsour.2013.05.099.
[3] Paknahad P, Askari M, Ghorbanzadeh M. Application of sol-gel technique to synthesis of copper-cobalt spinel on the ferritic stainless steel used for solid oxide fuel cell interconnects. J Power Sources 2014;266:79–87. http://dx.doi.org/10.1016/j.jpowsour.2014.04.122.
[4] Reddy AA, Eghtesadi N, Tulyaganov DU, Pascual MJ, Santos LF, Rajesh S, et al. Bi-layer glass-ceramic sealant for solid oxide fuel cells. J Eur Ceram Soc 2014;34:1449–55. http://dx.doi.org/10.1016/j.jeurceramsoc.2013.11.012.
[5] Kaur G, Pandey OP, Singh K. Chemical interaction study between lanthanum based different alkaline earth glass sealants with Crofer 22 APU for solid oxide fuel cell applications. Int J Hydrogen Energy 2012;37:3883–9. http://dx.doi.org/10.1016/j.ijhydene.2011.04.104.
[6] Lessing PA. A review of sealing technologies applicable to solid oxide electrolysis cells. J Mater Sci 2007;42:3465–76. http://dx.doi.org/10.1007/s10853-006-0409-9.

[7] Mahapatra MK, Lu K. Glass-based seals for solid oxide fuel and electrolyzer cells – a review. Mater Sci Eng R Rep 2010;67:65–85. http://dx.doi.org/10.1016/j.mser.2009.12.002.
[8] Fergus JW. Sealants for solid oxide fuel cells. J Power Sources 2005;147:46–57. http://dx.doi.org/10.1016/j.jpowsour.2005.05.002.
[9] Donald IW, Mallinson PM, Metcalfe BL, Gerrard LA, Fernie JA. Recent developments in the preparation, characterization and applications of glass- and glass–ceramic-to-metal seals and coatings. J Mater Sci 2011;46:1975–2000. http://dx.doi.org/10.1007/s10853-010-5095-y.
[10] Reddy AA, Tulyaganov DU, Pascual MJ, Kharton VV, Tsipis EV, Kolotygin VA, et al. Diopside–Ba disilicate glass–ceramic sealants for SOFCs: enhanced adhesion and thermal stability by Sr for Ca substitution. Int J Hydrogen Energy 2013;38:3073–86. http://dx.doi.org/10.1016/j.ijhydene.2012.12.074.
[11] Meinhardt KD, Kim D, Chou Y, Weil KS. Synthesis and properties of a barium aluminosilicate solid oxide fuel cell glass – ceramic sealant. J Power Sources 2008;182:188–96. http://dx.doi.org/10.1016/j.jpowsour.2008.03.079.
[12] Wu J, Liu X. Recent development of SOFC metallic interconnect. J Mater Sci Technol 2010;26:293–305. http://dx.doi.org/10.1016/S1005-0302(10)60049-7.
[13] Haanappel VAC, Shemet V, Gross SM, Koppitz T, Menzler NH, Zahid M, et al. Behaviour of various glass–ceramic sealants with ferritic steels under simulated SOFC stack conditions. J Power Sources 2005;150:86–100. http://dx.doi.org/10.1016/j.jpowsour.2005.02.015.
[14] Batfalsky P, Haanappel V a C, Malzbender J, Menzler NH, Shemet V, Vinke IC, et al. Chemical interaction between glass–ceramic sealants and interconnect steels in SOFC stacks. J Power Sources 2006;155:128–37. http://dx.doi.org/10.1016/j.jpowsour.2005.05.046.
[15] Stephens EV, Vetrano JS, Koeppel BJ, Chou Y, Sun X, Khaleel MA. Experimental characterization of glass – ceramic seal properties and their constitutive implementation in solid oxide fuel cell stack models. J Power Sources 2009;193:625–31. http://dx.doi.org/10.1016/j.jpowsour.2009.02.080.
[16] Thieme C, Rüssel C. Cobalt containing crystallizing glass seals for solid oxide fuel cells – a new strategy for strong adherence to metals and high thermal expansion. J Power Sources 2014;258:182–8. http://dx.doi.org/10.1016/j.jpowsour.2014.02.024.
[17] Chou Y-S, Thomsen EC, Choi J-P, Stevenson JW. Compliant alkali silicate sealing glass for solid oxide fuel cell applications: Combined stability in isothermal ageing and thermal cycling with YSZ coated ferritic stainless steels. J Power Sources 2012;197:154–60. http://dx.doi.org/10.1016/j.jpowsour.2011.09.027.
[18] Liu WN, Sun X, Khaleel MA. Study of geometric stability and structural integrity of self-healing glass seal system used in solid oxide fuel cells. J Power Sources 2011;196:1750–61. http://dx.doi.org/10.1016/j.jpowsour.2010.10.002.
[19] Chen J, Zou Q, Zeng F, Wang S, Tang D, Yang H, et al. Tailoring the sealing properties of TiO_2–CaO–SrO–B_2O_3–SiO_2 glass-ceramic seals: Thermal properties, chemical compatibility and electrical property. J Power Sources 2013;241:578–82. http://dx.doi.org/10.1016/j.jpowsour.2013.04.134.
[20] Kaur B, Singh K, Pandey OP. Microstructural study of Crofer 22 APU-glass interface for SOFC application. Int J Hydrogen Energy 2012;37:3839–47. http://dx.doi.org/10.1016/j.ijhydene.2011.04.160.
[21] Mantel M. Effect of double oxide layer on metal–glass sealing. J Non Cryst Solids 2000;273:294–301. http://dx.doi.org/10.1016/S0022-3093(00)00137-X.
[22] Zhang T, Zhang H, Li G, Yung H. Reduction of chromate formation at the interface of solid oxide fuel cells by different additives. J Power Sources 2010;195:6795–7. http://dx.doi.org/10.1016/j.jpowsour.2010.04.060.
[23] Coillot D, Méar FO, Nonnet H, Montagne L. New viscous sealing glasses for electrochemical cells. Int J Hydrogen Energy 2012;37:9351–8. http://dx.doi.org/10.1016/j.ijhydene.2012.02.194.
[24] Chou Y-S, Stevenson JW, Singh P. Effect of pre-oxidation and environmental aging on the seal strength of a novel high-temperature solid oxide fuel cell (SOFC) sealing glass with metallic interconnect. J Power Sources 2008;184:238–44. http://dx.doi.org/10.1016/j.jpowsour.2008.06.020.
[25] Smeacetto F, Salvo M, Ferraris M, Casalegno V, Asinari P. Glass and composite seals for the joining of YSZ to metallic interconnect in solid oxide fuel cells. J Eur Ceram Soc 2008;28:611–6. http://dx.doi.org/10.1016/j.jeurceramsoc.2007.07.008.
[26] Chou Y-S, Stevenson JW, Singh P. Effect of aluminizing of Cr-containing ferritic alloys on the seal strength of a novel high-temperature solid oxide fuel cell sealing glass. J Power Sources 2008;185:1001–8. http://dx.doi.org/10.1016/j.jpowsour.2008.09.004.
[27] Hsu J-H, Kim C-W, Brow RK. Interfacial interactions between an alkali-free borosilicate viscous sealing glass and aluminized ferritic stainless steel. J Power Sources 2014;250:236–41. http://dx.doi.org/10.1016/j.jpowsour.2013.11.018.
[28] Chou Y-S, Thomsen EC, Williams RT, Choi J-P, Canfield NL, Bonnett JF, et al. Compliant alkali silicate sealing glass for solid oxide fuel cell applications: Thermal cycle stability and chemical compatibility. J Power Sources 2011;196:2709–16. http://dx.doi.org/10.1016/j.jpowsour.2010.11.020.
[29] Chou Y-S, Stevenson JW, Choi J-P. Long-term evaluation of solid oxide fuel cell candidate materials in a 3-cell generic short stack fixture, Part II: sealing glass stability, microstructure and interfacial reactions. J Power Sources 2014;250:166–73. http://dx.doi.org/10.1016/j.jpowsour.2013.09.148.
[30] Nielsen KA, Solvang M, Nielsen SBL, Dinesen AR, Beeaff D, Larsen PH. Glass composite seals for SOFC application. J Eur Ceram Soc 2007;27:1817–22. http://dx.doi.org/10.1016/j.jeurceramsoc.2006.05.046.
[31] Choi JP, Scott Weil K, Matt Chou Y, Stevenson JW, Gary Yang Z. Development of MnCoO coating with new aluminizing process for planar SOFC stacks. Int J Hydrogen Energy 2011;36:4549–56. http://dx.doi.org/10.1016/j.ijhydene.2010.04.110.
[32] Chou Y-S, Stevenson JW, Xia G-G, Yang Z-G. Electrical stability of a novel sealing glass with (Mn,Co)-spinel coated Crofer22APU in a simulated SOFC dual environment. J Power Sources 2010;195:5666–73. http://dx.doi.org/10.1016/j.jpowsour.2010.03.052.
[33] Chou Y-S, Thomsen EC, Choi J-P, Stevenson JW. Compliant alkali silicate sealing glass for solid oxide fuel cell applications: the effect of protective YSZ coating on electrical stability in dual environment. J Power Sources 2012;202:149–56. http://dx.doi.org/10.1016/j.jpowsour.2011.11.017.
[34] Chou Y-S, Stevenson JW, Choi J-P. Long-term evaluation of solid oxide fuel cell candidate materials in a 3-cell generic stack test fixture, part III: stability and microstructure of Ce-(Mn,Co)-spinel coating, AISI441 interconnect, alumina coating, cathode and anode. J Power Sources 2014;257:444–53. http://dx.doi.org/10.1016/j.jpowsour.2013.11.086.
[35] Nielsen KA, Solvang M, Nielsen SBL, Beeaff D. Mechanical behaviour of glassy composite seals for IT-SOFC application.

J Ceram Eng Sci 2008;27:315–23. http://dx.doi.org/10.1002/9780470291337.ch31.
[36] Mahapatra MK, Lu K. Seal glass compatibility with bare and $(Mn,Co)_3O_4$ coated AISI 441 alloy in solid oxide fuel/electrolyzer cell atmospheres. Int J Hydrogen Energy 2010;35:11908–17. http://dx.doi.org/10.1016/j.ijhydene.2010.08.066.
[37] Widgeon SJ, Corral EL, Spilde MN, Loehman RE. Glass-to-metal seal interfacial analysis using electron probe microscopy for reliable solid oxide fuel cells. J Am Ceram Soc 2009;786:781–6. http://dx.doi.org/10.1111/j.1551-2916.2008.02902.x.
[38] Shong W-J, Liu C-K, Yang P. Effects of electroless nickel plating on 441 stainless steel as SOFC interconnect. Mater Chem Phys 2012;134:670–6. http://dx.doi.org/10.1016/j.matchemphys.2012.03.049.
[39] Fu C, Sun K, Chen X, Zhang N, Zhou D. Effects of the nickel-coated ferritic stainless steel for solid oxide fuel cells interconnects. Corros Sci 2008;50:1926–31. http://dx.doi.org/10.1016/j.corsci.2008.05.001.
[40] Nielsen KA, Dinesen AR, Korcakova L, Mikkelsen L, Hendriksen PV, Poulsen FW. Testing of Ni-plated ferritic steel interconnect in SOFC stacks. Fuel Cells 2006;6:100–6. http://dx.doi.org/10.1002/fuce.200500114.
[41] Leonard ME, Amendola R, Gannon PE, Shong W-J, Liu C-K. High-temperature (800 °C) dual atmosphere corrosion of electroless nickel-plated ferritic stainless steel. Int J Hydrogen Energy 2014;39:15746–53. http://dx.doi.org/10.1016/j.ijhydene.2014.07.144.
[42] Wainer E, Baldwin WJ. Nickel flashing and it's relation to enamel adherence. J Am Ceram Soc 1945;28:317–26. http://dx.doi.org/10.1111/j.1151-2916.1945.tb14501.x.
[43] Crystal H, Bullock G. Oxide adherence and nickel flashing in vitreous enameling. J Am Ceram Soc 1959;42:30–9. http://dx.doi.org/10.1111/j.1151-2916.1959.tb09139.x.
[44] Eppler RA, Eppler DR. Glazes and glazes coating. Hong Kong: The American Ceramic Society; 2000.
[45] Chou Y-S, Choi J-P, Stevenson JW. Compliant alkali silicate sealing glass for solid oxide fuel cell applications: the effect of protective alumina coating on electrical stability in dual environment. Int J Hydrogen Energy 2012;37:18372–80. http://dx.doi.org/10.1016/j.ijhydene.2012.08.084.
[46] EN 10209. Cold-rolled low carbon steel flat products for vitreous enameling-Technical delivery conditions. 1996.
[47] ImageJ. Available: http://imagej.nih.gov/ij/.
[48] Smeacetto F, Salvo M, Ferraris M, Casalegno V, Asinari P, Chrysanthou A. Characterization and performance of glass–ceramic sealant to join metallic interconnects to YSZ and anode-supported-electrolyte in planar SOFCs. J Eur Ceram Soc 2008;28:2521–7. http://dx.doi.org/10.1016/j.jeurceramsoc.2008.03.035.
[49] Smeacetto F, Chrysanthou A, Salvo M, Zhang Z, Ferraris M. Performance and testing of glass-ceramic sealant used to join anode-supported-electrolyte to Crofer22APU in planar solid oxide fuel cells. J Power Sources 2009;190:402–7. http://dx.doi.org/10.1016/j.jpowsour.2009.01.042.
[50] Xiong W. Thermodynamic and kinetic investigation of the Fe–Cr–Ni system driven by engineering applications. KHT Royal Institute of technology; 2012.
[51] Yang X, Jha A, Brydson R, Cochrane R. The effects of a nickel oxide precoat on the gas bubble structures and fish-scaling resistance in vitreous enamels. Mater Sci Eng A 2004;366:254–61. http://dx.doi.org/10.1016/j.msea.2003.08.003.
[52] Paul A. Chemistry of glasses. 2nd ed. London: Chapman and Hall; 1990.
[53] Chen S, Lin J, Yang H, Tang D, Zhang T. Controlling the redox reaction at the interface between sealing glasses and Cr-containing interconnect: effect of competitive reaction. J Power Sources 2014;267:753–9. http://dx.doi.org/10.1016/j.jpowsour.2014.06.004.
[54] Ling G, He J. The influence of nano-Al_2O_3 additive on the adhesion between enamel and steel substrate. Mater Sci Eng A 2004;379:432–6. http://dx.doi.org/10.1016/j.msea.2004.03.019.
[55] Bodaghi M, Davarpanah A. The influence of cobalt on the microstructure and adherence characteristics of enamel on steel sheet. Process Appl Ceram 2011;5:215–22. http://dx.doi.org/10.2298/PAC1104215B.
[56] Abdullah TK, Petitjean C, Panteix P-J, Rapin C, Vilasi M, Hussain Z, et al. Dissolution equilibrium of chromium oxide in a soda lime silicate melt exposed to oxidizing and reducing atmospheres. Mater Chem Phys 2013;142:572–9. http://dx.doi.org/10.1016/j.matchemphys.2013.07.055.
[57] Kumar V, Kaur G, Pandey OP, Singh K, Lu K. Effect of thermal treatment on chemical interaction between yttrium borosilicate glass sealants and YSZ for planar solid oxide fuel cells. Int J Appl Glas Sci 2014;5:1–11. http://dx.doi.org/10.1111/ijag.12078.
[58] Menzler NH, Sebold D, Zahid M, Gross SM, Koppitz T. Interaction of metallic SOFC interconnect materials with glass–ceramic sealant in various atmospheres. J Power Sources 2005;152:156–67. http://dx.doi.org/10.1016/j.jpowsour.2005.02.072.
[59] Kaur G, Pandey OP, Singh K. Interfacial study between high temperature SiO_2–B_2O_3–AO–La_2O_3 (A = Sr, Ba) glass seals and Crofer 22APU for solid oxide fuel cell applications. Int J Hydrogen Energy 2012;37:6862–74. http://dx.doi.org/10.1016/j.ijhydene.2012.01.118.
[60] Di Martino J, Rapin C, Berthod P, Podor R, Steinmetz P. Corrosion of metals and alloys in molten glasses. Part 1: glass electrochemical properties and pure metal (Fe, Co, Ni, Cr) behaviours. Corros Sci 2004;46:1849–64. http://dx.doi.org/10.1016/j.corsci.2003.10.024.